Thermally induced surface instability in ion-implanted $Mg_xZn_{1-x}O$ films

A. Yu. Azarov,[1] A. Hallén,[2] X. L. Du,[3] Z. L. Liu,[3] B. G. Svensson,[1] and A. Yu. Kuznetsov[1]
[1] *Department of Physics, University of Oslo, P.O. Box 1048, Blindern, NO-0316 Oslo, Norway*
[2] *ICT-MAP, Royal Institute of Technology, Electrum 229, SE-164 40, Kista-Stockholm, Sweden*
[3] *Institute of Physics, The Chinese Academy of Sciences, Beijing 100190, China*
(Received 5 November 2010; revised manuscript received 2 May 2011; published 28 July 2011)

Thermal stability of originally single crystalline wurtzite $Mg_xZn_{1-x}O$ ($x \leqslant 0.3$) films implanted at room temperature with ^{166}Er ions is studied by a combination of Rutherford backscattering spectrometry, time-of-flight elastic recoil detection analysis, x-ray diffraction analysis, and atomic force microscopy. The MgZnO films exhibit a complex behavior during postimplantation annealing associated with compositional changes and surface erosion in addition to Er accumulation at the surface. The importance of these processes depends on the Mg content, annealing temperature, and amount of implantation damage. Specifically, increases in the Mg content as well as the implantation damage enhance the compositional changes in the near-surface region and give rise to altered stoichiometry and Mg-enriched phase separation. In its turn, the rate of surface erosion in MgZnO under the thermal treatment depends on temperature, MgZnO composition, and the amount of implantation damage nontrivially, which is attributed to the compositional changes in the near-surface region assisted by the implantation damage.

DOI: 10.1103/PhysRevB.84.014114 PACS number(s): 68.60.Dv, 61.72.Cc

I. INTRODUCTION

In recent years there has been steadily growing interest in ZnO-based ternary oxides.[1–9] This research interest has been stimulated by promising possibilities of utilization of such materials in optoelectronics covering a broad spectral range. Specifically, ZnO is a wide direct band-gap ($E_g \approx 3.3$ eV) semiconductor, but alloying it with MgO ($E_g \approx 7.8$ eV) results in the band-gap being tuned, for example, to the so-called solar-blind spectral region.[10] However, MgO and ZnO have different crystal structures: ZnO has a hexagonal wurtzite structure under normal conditions, while MgO has a rock-salt cubic structure. Moreover, the thermodynamic solid solubility of MgO in ZnO is relatively low,[7,11] and fabrication of high-quality wurtzite MgZnO alloys with high Mg content has been demonstrated employing metastable growth conditions only.[3] Thus, the crystalline quality of MgZnO films and, hence, their utilization for optical devices are challenged by phase separation at high Mg contents.[3,7,9]

Doping by ion implantation is attractive for fabrication of electronic devices. The main drawback of ion implantation is, however, that the energetic ions inevitably produce defects that adversely affect device performance. Postimplantation annealing is, therefore, instrumental to remove the ion-induced defects and to activate the dopants. However, postimplantation annealing of metastable MgZnO may distort the material, and additional complications come from the fact that, even for pure ZnO, the mechanisms of damage formation and annealing are poorly understood. It has been shown that in heavy ion–implanted ZnO, the damage accumulates both in the crystal bulk and in the vicinity of the surface.[12] Furthermore, the "bulk" disorder saturates with increasing ion dose, and the damage accumulation exhibits an anomalous multipeak distribution when high-density collision cascades are generated.[12,13] In addition, annealing of the damage is often complicated by a surface degradation, caused by oxygen loss and change in material composition at high temperature ($\geqslant$1000 °C).[14,15] In fact, changes in the surface morphology have been observed already after low-temperature anneals (>200 °C in nitrogen ambient environment and >300 °C in air), featured with an increased surface roughness.[14] These effects are likely to become even more pronounced when applying the high ion doses required to accomplish heavily doped regions.[15]

The thermal stability of MgZnO films is less studied than that of pure ZnO. A major part of the existing reports deals with the effect of annealing on structural instability of as-grown MgZnO films without addressing the role of the surface.[6–8] In particular, it has been found that the thermal stability/degradation of as-grown MgZnO films may be controlled by phase separation,[6–8] and segregation of MgO in MgZnO films has been observed to occur already at 850 °C for high enough Mg content.[6] However, the way in which the surface and ion-induced defects affect the thermal stability/degradation of MgZnO films has not been documented. In the present work, we address these issues and study Er ion-implanted MgZnO films with different Mg contents (0 to 30%). Two fundamental processes—compositional changes and erosion—occurring at, or in the vicinity of, the surface are found to limit the thermal stability of MgZnO. The importance of these processes depends on the Mg content, annealing temperature, and ion dose.

II. EXPERIMENTAL METHODS

About 1-μm-thick wurtzite (0001) $Mg_xZn_{1-x}O$ ($x = 0, 0.1,$ and 0.3) layers were grown by molecular beam epitaxy (MBE) on sapphire substrates employing thin ZnO buffer layers. According to x-ray diffraction (XRD) analysis, all as-grown MgZnO samples exhibited single-phase wurtzite structure without any indication of phase separation. The samples were implanted at room temperature with 150 keV $^{166}Er^+$ ions using a flux of 2.5×10^{12}cm^{-2} s^{-1} and a dose range of 1×10^{15}–3×10^{16}cm^{-2}. The projected range of 150 keV $^{166}Er^+$ ions in pure ZnO is estimated to be ~32 nm, according to TRIM code[16] simulation, and all the implantations were carried out at 7° off

 ©2011 American Physical Society

the [0001] direction in order to minimize channeling. After the implantations, the samples were annealed at 700, 800, and 900 °C for 30 min in a vacuum. As-grown MgZnO samples were also annealed at the same conditions to discriminate between implantation-induced effects and pure thermal ones. In addition, the as-grown $Mg_{0.3}Zn_{0.7}O$ sample was annealed at 900 °C for 30 min in ambient oxygen.

The damage evolution was analyzed by Rutherford backscattering/channeling spectrometry (RBS/C) with 2 MeV $^4He^+$ ions incident along the [0001] direction and backscattered into detectors positioned at 170° and 100° relative to the incident beam direction. The 100°, so-called glancing-angle detector, geometry was used to provide enhanced depth resolution for examining near-surface damage accumulation. The 170° geometry was used to provide enhanced mass resolution to accurately examine the material's composition over the whole film thickness.

In addition to RBS, the elemental depth profiles of the films were measured with time-of-flight elastic recoil detection analysis (ToF-ERDA), which is more sensitive for detection of light elements than RBS.[17] The ToF-ERDA was performed using 40 MeV $^{127}I^{8+}$ ions. The incoming ions/outgoing recoils impinged/exited at 67.5° relative to the sample surface normal, giving a recoil angle of 45°. Analyses of the raw recoil ToF-ERDA data were done using the CONTES code.[18]

The surface roughness was studied by tapping mode atomic force microscopy (AFM) using a Veeco Nanoscope Dimension 3000 setup, while XRD analysis was performed using a D8 Bruker setup to reveal phase separation in the films.

III. RESULTS AND DISCUSSION

A. Surface decomposition

Figure 1 shows channeling and random RBS spectra of (a) pure ZnO, (b) $Mg_{0.1}Zn_{0.9}O$, and (c) $Mg_{0.3}Zn_{0.7}O$ films implanted with 150 keV $^{166}Er^+$ ions to a dose of 2×10^{15}cm^{-2} and films also subjected to postimplantation anneals at 800 and 900 °C. The arrows in Fig. 1(c) indicate the surface position of signals obtained from different elements present in the samples. As seen from the channeling spectrum of as-implanted pure ZnO sample (Fig. 1(a)), the damage-depth profile is characterized by two distinct peaks: the "bulk" peak, with the maximum roughly at channel no. 290, and the "surface" peak. Such bimodal damage accumulation behavior is consistent with previous studies of the damage buildup in ZnO implanted with heavy ions.[12] This bimodality weakens in $Mg_{0.1}Zn_{0.9}O$ and practically disappears in $Mg_{0.3}Zn_{0.7}O$ (Fig. 1(b) and 1(c)); this was recently interpreted as a retardation of dynamic annealing and/or effects of phase separation in the region between the bulk damage peak and the film surface of MgZnO (Ref. 19). The yield from the immediate surface region remains essentially constant for the three types of films, and the counts for channel nos. larger than ~325 are due to the implanted Er atoms, discussed in Sec. III D.

Figure 1 reveals also that annealing at 800 °C reduces the amount of damage, and the depth distribution becomes unimodal, possibly because of a strong recovery of the crystal structure in the vicinity of the surface. Further annealing at 900 °C of ZnO and $Mg_{0.1}Zn_{0.9}O$ leads to almost complete

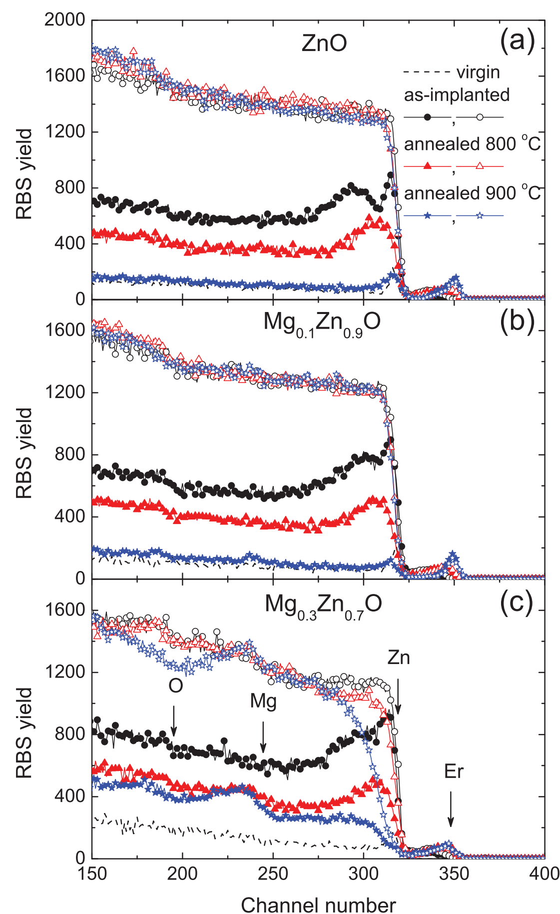

FIG. 1. (Color online) Random (open symbols) and channeling (closed symbols) RBS spectra (acquired with 100° detector geometry) of (a) ZnO, (b) $Mg_{0.1}Zn_{0.9}O$, and (c) $Mg_{0.3}Zn_{0.7}O$ implanted with 150 keV Er ions to 2×10^{15}cm^{-2} and annealed at 800 and 900 °C for 30 min. The positions of Zn, Mg, O, and Er atoms at the film surface are indicated by corresponding arrows in panel (c). Dashed lines represent channeling spectra taken from as-grown samples.

recovery of the crystal structure, and the channeling spectra resemble the virgin ones, especially in pure ZnO (Fig. 1(a)). However, this apparent restoration of crystallinity is attributed to the erosion of the surface rather than to damage recovery, as discussed in detail in Sec. III C. Note that the shape of the random spectra reveals no, or only minor, changes after the thermal treatment, suggesting negligible stoichiometric changes.

In contrast, the $Mg_{0.3}Zn_{0.7}O$ film exhibits dramatically different behavior compared to the two previous films (Fig. 1(c)). Already at 800 °C annealing gives rise to a significant difference in the near-surface region compared with the as-implanted state (see the random spectra), and the difference becomes even more pronounced after annealing at 900 °C. A straightforward interpretation of the different random spectra in Fig. 1(c) is a decrease of the Zn content near the surface in the $Mg_{0.3}Zn_{0.7}O$ films. Another interesting feature unveiled by Fig. 1(c) is the increased yield in two regions of the channeling spectrum (channels 160–180 and 220–250) for the sample annealed at 900 °C; the positions of these regions correspond to signals from O and Mg atoms located close to the surface.

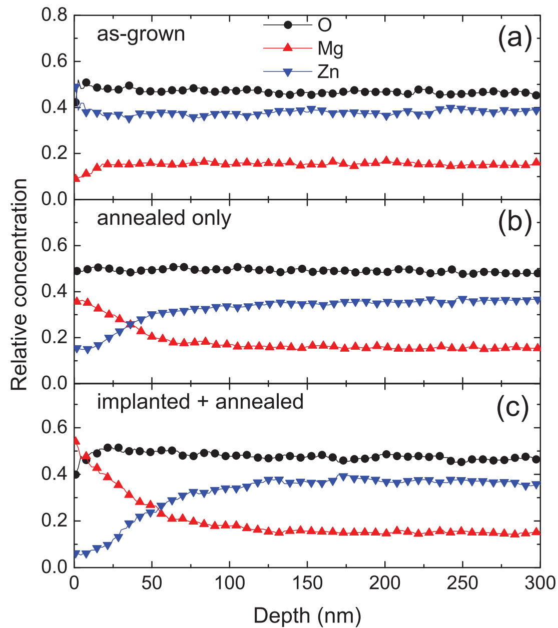

FIG. 2. (Color online) The depth profiles (extracted from ToF-ERDA spectra) of relative concentration of Zn, O, and Mg atoms in $Mg_{0.3}Zn_{0.7}O$ (a) as-grown, (b) annealed at 900 °C, and (c) implanted with 150 keV Er ions to $2 \times 10^{15} cm^{-2}$ and subsequently annealed at 900 °C.

In addition, the increased yield for the random spectrum of the 900 °C annealed sample in the channels 220–250 strongly indicates a Mg pile-up at the surface.

The interpretation given above is supported by ToF-ERDA results, which are summarized in Fig. 2, showing the Zn, O, and Mg elemental-depth profiles for (a) as-grown, (b) annealed only, (c) implanted and annealed $Mg_{0.3}Zn_{0.7}O$ samples.[20] Figure 2(c) demonstrates that postimplantation annealing at 900 °C decreases the Zn content near the surface with a symmetric increase in the Mg content, which reaches ∼0.5 at the film surface. Importantly, annealing of the corresponding as-grown sample (Fig. 2(b)) leads to smaller compositional changes, and it can be concluded that implantation damage promotes changes in the surface composition, as is further investigated in Sec. III B for different ion doses. The O concentration profiles in Fig. 2 remain practically unaffected for the different samples; this implies that the Mg atoms preferentially substitute for the Zn atoms, forming MgO and/or Mg-rich MgZnO clusters in the vicinity of the surface. Formation of metallic Mg clusters appears to be less likely.

The data in Figs. 1 and 2 show that the $Mg_{0.3}Zn_{0.7}O$ films are not stable, and the most pronounced stoichiometric changes occur in the near-surface region during high-temperature postimplantation annealing. These effects are less pronounced in the $Mg_{0.1}Zn_{0.9}O$ films; this is natural if the process is governed by the difference in crystal structure and low solid solubility of MgO in ZnO, such that a larger wurtzite/cubic phase separation takes place with increasing temperature and Mg content.[21] The process appears also to be enhanced by the implantation-induced defects, and the increased yield in the channeling spectrum (channels 220–250 and 160–180) of the annealed $Mg_{0.3}Zn_{0.7}O$ sample (Fig. 1(c)) can be attributed to defect-assisted phase separation with segregation of MgO in the near-surface region. Furthermore, it is well known that ZnO forms a Zn-rich (O-deficient) surface layer when treated at high temperatures in an ambient-like vacuum.[14,15] Zn has relatively low melting and boiling temperatures, ∼420 and ∼910 °C, respectively,[22] while the corresponding ones for Mg are significantly higher, ∼650 and ∼1100 °C, respectively.[22] Thus, it is likely that the surface of MgZnO is enriched with Mg at the expense of Zn during annealing at high temperature.

The interpretation of a thermally induced phase separation of the implanted MgZnO films is also corroborated by the XRD results, as shown in Fig. 3, which shows 2Θ scans of as-grown and processed $Mg_{0.3}Zn_{0.7}O$ samples. Characteristic peaks at 34.6° and 41.7° are revealed in all samples and attributed to the wurtzite MgZnO and the sapphire substrate, respectively. In addition, an extra peak at ∼42.7° emerges in the annealed samples corresponding to the (200) rock-salt MgO reflection, strongly suggesting phase separation with segregation of pure MgO and/or a cubic Mg-rich MgZnO phase. The intensity of the 42.7° peak is very weak in the annealed-only sample, supporting the scenario of implantation-induced enhancement of changes in the film composition, as discussed previously for the RBS and ERDA data. Moreover, it is seen that this peak is almost undistinguishable in the unimplanted sample annealed in ambient oxygen, giving, together with the results shown in Figs. 1 and 2, a strong indication that the Mg-rich cubic phase formation occurs preferentially in the near-surface region, presumably related to the changes in film composition occurring during vacuum annealing, as discussed above. It should be emphasized that the full-width-half-maximum (FWHM) of the wurtzite-related peak in the posimplant annealed sample increases in comparison with that in the as-implanted sample, indicating that the annealing leads to an overall degradation of the crystalline quality of the film.

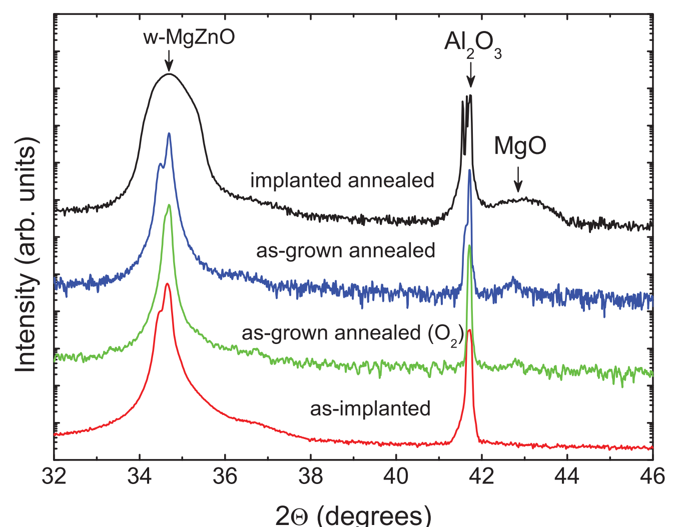

FIG. 3. (Color online) Typical XRD 2Θ scans of $Mg_{0.3}Zn_{0.7}O$ films implanted by 150 keV Er ions to $2 \times 10^{15} cm^{-2}$ before and after annealing at 900 °C in a vacuum. The XRD spectra of unimplanted samples annealed at 900 °C in vacuum and ambient oxygen are also shown for comparison.

B. High-dose effects

Figure 4 illustrates the structural evolution upon annealing in (a) pure ZnO and (b) $Mg_{0.3}Zn_{0.7}O$ implanted with the highest ion dose used (3×10^{16} Er/cm^2). The crystal structure of pure ZnO is substantially recovered already after the 700 °C annealing (Fig. 4(a)), which is in fact attributed to a strong surface erosion and thinning of the heavily damaged ZnO film, as shown in Sec. III C. This result is consistent with previous studies of thermal stability of heavily damaged ZnO, see, e.g., Coleman *et al.*,[15] and it supports the trend of lower thermal stability of ZnO with increasing amount of ion-induced damage. Note that further annealing at 800 °C does not change the shape of the RBS/C spectra, and, for simplicity, these results are not shown. In contrast to pure ZnO, similar anneals of heavily implanted $Mg_{0.3}Zn_{0.7}O$ (see, e.g., 700 °C in Fig. 4(b)) demonstrate practically no effect on the overall amount of damage. Instead, the anneals result in strong stoichiometry changes near the surface, which become dramatic after the 800 °C anneal (Fig. 4(b)). Compared with the data in Fig. 1(c) (2×10^{15} Er/cm^2) for the 800 °C anneal, it is evident that the structural changes in the near-surface region are much more pronounced in Fig. 4(b). Hence, this result provides additional evidence that implantation-induced damage affects the surface composition of MgZnO films during postimplantation annealing.

C. Surface erosion

The changes in surface composition revealed by Figs. 1–4 are accompanied by film erosion, as confirmed by Fig. 5, which

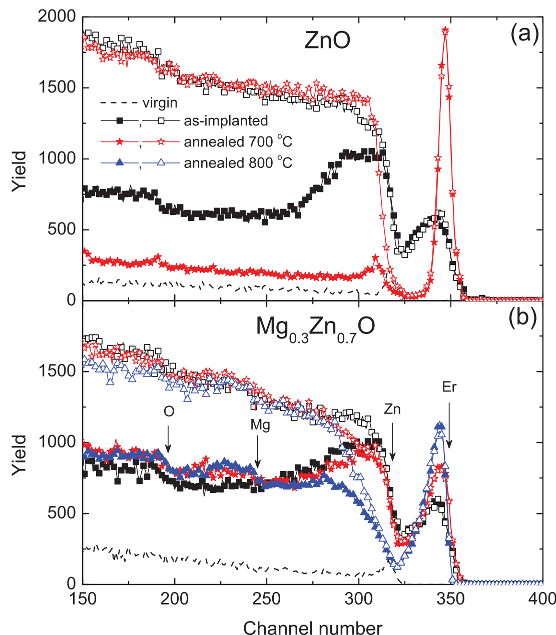

FIG. 4. (Color online) Random (open symbols) and channeling (closed symbols) RBS spectra (acquired with 100° detector geometry) of (a) ZnO and (b) $Mg_{0.3}Zn_{0.7}O$ films implanted with 150 keV Er^+ ions to $3 \times 10^{16} cm^{-2}$ before and after annealing at 700 °C and 800 °C (shown for the $Mg_{0.3}Zn_{0.7}O$ only). The dashed lines represent channeling spectra taken from as-grown samples. The positions of Zn, Mg, O, and Er at the film surface are indicated by corresponding arrows in panel (b).

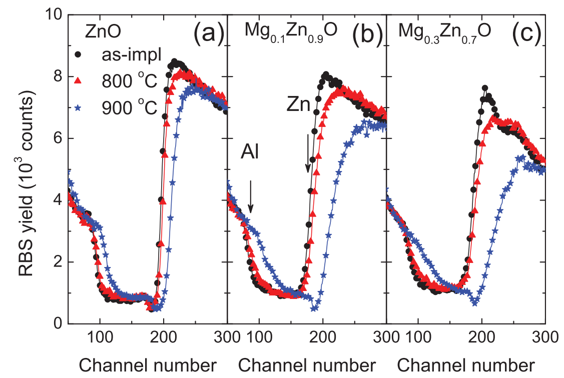

FIG. 5. (Color online) Portions of random RBS spectra (acquired with 170° detector geometry) corresponding to the substrate/film depth range in (a) ZnO, (b) $Mg_{0.1}Zn_{0.9}O$, and (c) $Mg_{0.3}Zn_{0.7}O$ samples implanted with 150 keV Er^+ ions to $2 \times 10^{15} cm^{-2}$ and annealed at 800 and 900 °C. The positions of Al and Zn at the initial film/substrate interface are indicated in panel (b) by the arrows.

shows fragments of the random RBS spectra in the vicinity of the film/substrate interface for some selected samples. The position of Al and Zn atoms at the initial interface is indicated by the arrows in Fig. 5(b), and annealing leads to a systematic shift of the corresponding spectral signatures to higher channel numbers (most pronounced at 900 °C). Furthermore, Fig. 5 reveals that the slope of the spectrum edges, which corresponds to the abruptness of film/substrate interface, decreases with annealing. The shift increases with increasing Mg content and is primarily attributed to a reduction of the film thickness (surface erosion). However, partial contributions to the shift arise also from the degradation of film/substrate interface and the modified surface region with altered stoichiometry, which affects the stopping power of the analyzing He ions. The degradation of the film/substrate interface during annealing is presumably due to intermixing of Zn, Mg, and Al atoms.[23,24]

Note that the observed changes in the slopes of the spectra are not caused by roughening of the surface; despite the fact that the high-temperature annealing leads to a significant surface modification (in terms of composition and erosion), the increase in the surface roughness is rather modest, as illustrated by the AFM results in Fig. 6. The erosion revealed in Fig. 5 is at least one order of magnitude higher than the values of the surface roughness in Fig. 6. Moreover, the variations with annealing observed in Fig. 6 are practically independent on the film composition and exhibit no correlation with the interfacial broadening found in Fig. 5.

The data in Fig. 5 (and similar measurements for the rest of the samples) were employed to estimate the amount of the removed material based on the shift of the Zn position at the film/substrate interface in the spectra. The results are shown in Fig. 7, which summarizes the effects of ion dose and Mg content. It is seen from Fig. 7(a) that the surface erosion increases with increasing ion dose or the amount of implantation damage.[25] Furthermore, comparing the data at 900 °C (Fig. 7(b)) for the samples annealed only and the samples implanted plus annealed, it is seen that the surface erosion is about a factor of two higher in the latter samples, even for the low implantation dose. This holds irrespective of

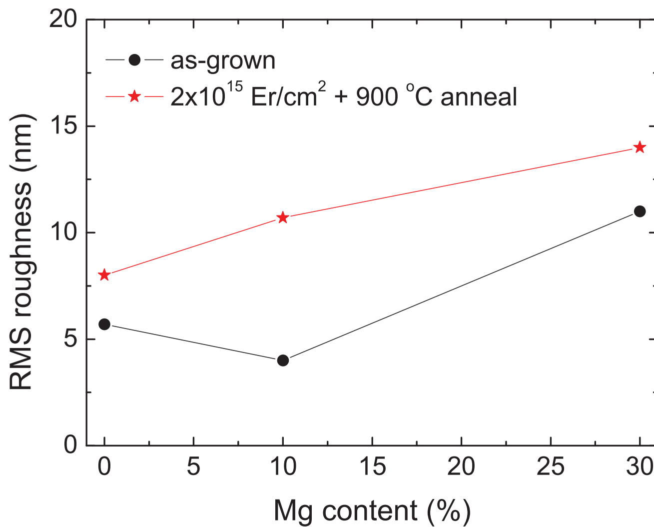

FIG. 6. (Color online) Surface roughness (measured by AFM) as a function of the Mg content in as-grown (dots) and processed (stars) $Mg_xZn_{1-x}O$ samples.

the Mg content, but the absolute values increase with the Mg content. However the rate of surface erosion depends on Mg content and implanted dose nontrivially. Indeed, at 700 °C and for the highest Er dose used (3×10^{16} cm^{-2}), an opposite trend occurs, where the surface erosion decreases with increasing Mg content (see Fig. 7(b)). This behavior is perhaps surprising but can be attributed to a rapid defect-assisted accumulation of Mg in the near-surface region during postimplantation annealing for the high-dose sample (containing a high concentration of ion-induced defects). As discussed in Sec. III A, such a modified surface layer is anticipated to be more thermally stable than a pure ZnO layer, and the surface erosion is retarded.

D. Er distribution

Figure 8 shows the concentration versus depth profiles of Er, deduced from random RBS spectra, in pure ZnO implanted with different doses. Up to a dose of 1×10^{16} cm^{-2}, the measured profiles (symbols) are in good agreement with simulations using the TRIM code[26] (dashed lines in Fig. 8). However, for a dose of 3×10^{16} cm^{-2}, the profiles deviate, where the measured one is located closer to the surface and exhibits a more positive skewness than the simulated one. Similar trends are also observed for the as-implanted MgZnO samples (not shown). These deviations at high Er doses may arise from either sputtering of the films or/and altering of the stopping power in the near-surface region due to the large amount of Er atoms introduced (which was not accounted for in the TRIM simulations).

It is possible to estimate the substitutional fraction of Er atoms by comparing the depth profiles obtained under random and channeling conditions. The results of such analysis for the as-implanted layers are shown in the inset of Fig. 8, demonstrating a decrease with increasing dose, irrespective of the Mg content. However, for a given dose, the substitutional fraction appears to decrease with increasing Mg content.

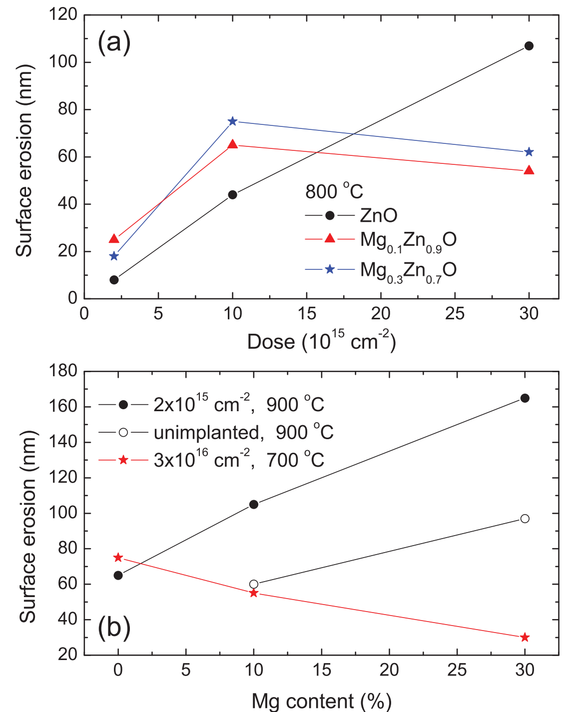

FIG. 7. (Color online) Surface erosion or amount of the material removed (a) in 800 °C annealed $Mg_xZn_{1-x}O$ as a function of ion dose and (b) in the $Mg_xZn_{1-x}O$ samples subjected to different processing as indicated in the legend as a function of the Mg content.

The behavior of Er during annealing can be traced from Fig. 4. Annealing of the heavily implanted pure ZnO films shifts the Zn surface edge to lower channels, accompanied with a sharpening of the Er peak (Fig. 4(a)), strongly indicating segregation of Er at the sample surface. Interestingly, no loss of Er occurs in spite of a surface erosion of ∼75 nm (Fig. 7). Annealing of lower-dose implanted pure ZnO films

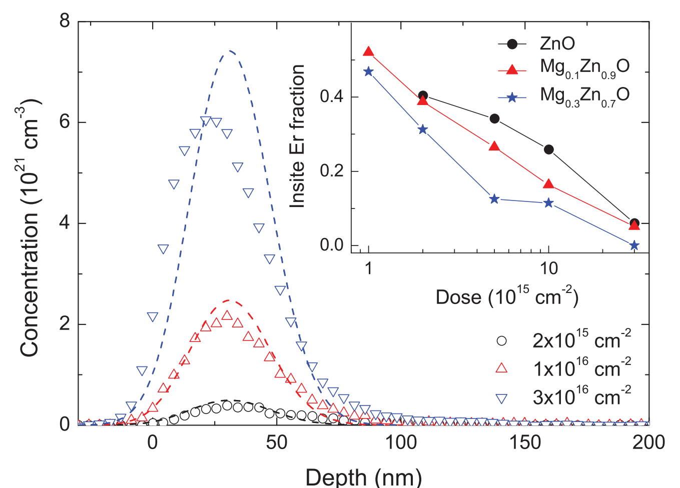

FIG. 8. (Color online) Er concentration vs depth profiles (open symbols) in ZnO implanted with 150 keV Er ions to different ion doses as indicated in the legend. The corresponding Er depth profiles predicted[26] theoretically are shown by the dashed lines. The inset plots the substitutional fraction of Er atoms as a function of the implanted dose in the samples having different Mg content.

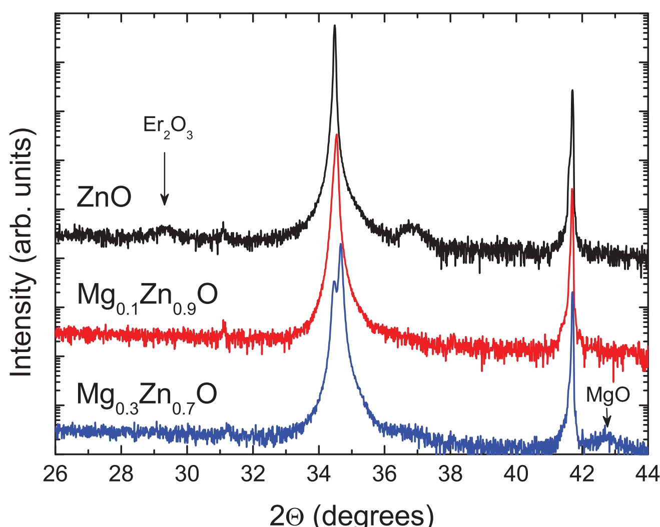

FIG. 9. (Color online) Typical XRD 2Θ scans taken from $Mg_xZn_{1-x}O$ films implanted by 150 keV Er ions to $3 \times 10^{16} cm^{-2}$ and subjected to annealing at 800 °C.

(not shown) gives rise to similar trends as in Fig. 4(a). In this context, it should be pointed out that the apparent damage recovery accompanied with dopant segregation at the surface reported previously in literature[27,28] for annealed ZnO samples implanted with rare earth ions may be attributed to surface erosion similar to that observed in Fig. 5(a). These findings emphasize the importance of film stability for the interpretation of RBS/C results.

Annealing of the MgZnO films is characterized by less pronounced Er redistribution compared to that in pure ZnO, as illustrated by Fig. 4(b) for the $Mg_{0.3}Zn_{0.7}O$ films, and accumulation at the surface is much weaker with a broad Er peak. This difference may be due to a low diffusivity of Er in $Mg_{0.3}Zn_{0.7}O$, but also chemical effects can play a role. Figure 9 shows XRD spectra of samples implanted with 3×10^{16} Er/cm^2 and annealed at 800 °C, and two distinct features deserve attention. First, pure ZnO displays a peak at ∼29.3°, which corresponds closely to a reflection from the Er_2O_3 phase[29] and indicates erbium-oxide formation at the ZnO surface rather than segregation of metallic Er. Second, the 29.3° peak is not observed in the $Mg_{0.3}Zn_{0.7}O$ sample, where another peak emerges at ∼42.7°, corresponding to a cubic MgO phase (as discussed in Sec. III D). Hence, the limited Er redistribution in MgZnO may arise from a competition between MgO and Er_2O_3 formation at the surface.

IV. SUMMARY AND CONCLUSIONS

In summary, the thermally induced surface instability in MgZnO films implanted with heavy Er^+ ions was investigated. It is found that the thermal degradation of implanted MgZnO films is a complex process involving the interplay/competition of phenomena of surface decomposition, phase separation, surface erosion, and dopant redistribution. The efficiency of these phenomena depends on Mg content and amount of implantation damage. In particular, implantation damage facilitates the processes of surface decomposition and material evaporation at a given temperature. Concurrently with these processes, the implanted Er atoms may segregate at the surface with erbium-oxide formation.

The processes of phase separation and the different capabilities to evaporate of Mg and Zn atoms should be taken into account when the thermal degradation of MgZnO is considered. These effects lead to Mg/Zn pile-up/depletion and a Mg-enriched cubic phase formation near the surface. In its turn, this new Mg-enriched MgZnO phase can suppress both further material removal and Er redistribution due to chemical effects and higher thermal stability of MgO compared to that of pure ZnO. These effects may be responsible for the experimentally observed nontrivial dependence of the surface erosion rate in MgZnO on the Mg content and the amount of implantation damage, where for low-dose implantation, the surface erosion enhances with increasing Mg content, while exhibiting an opposite trend for the high-dose implants.

ACKNOWLEDGMENTS

The authors acknowledge Jens Jensen and Tianchong Zhang for their assistance with some of the ToF-ERDA and XRD measurements, respectively. Financial support from the Research Council of Norway via FRINAT and RENERGI programs is gratefully acknowledged. The international cooperation was partially funded by NordForsk, NSFC (61076007 & 50532090) and MOSTC (2011CB302002 & 2007CB936203).

[1] Ü. Özgür, Ya. I. Alivov, C. Liu, A. Teke, M. A. Reshchikov, S. Doğan, V. Avrutin, S.-J. Cho, and H. Morkoç, J. Appl. Phys. **98**, 041301 (2005).

[2] T. Makino, Y. Segawa, M. Kawasaki, A. Ohtomo, R. Shiroki, K. Tamura, T. Yasuda, and H. Koinuma, Appl. Phys. Lett. **78**, 1237 (2001).

[3] Z. L. Liu, Z. X. Mei, T. C. Zhang, Y. P. Liu, Y. Guo, X. L. Du, A. Hallen, J. J. Zhu, and A. Yu. Kuznetsov, J. Cryst. Growth **311**, 4356 (2009).

[4] J. W. Kim, H. S. Kang, J. H. Kim, S. Y. Lee, J.-K. Lee, and M. Nastasi, J. Appl. Phys. **100**, 033701 (2006).

[5] H.-C. Hsu, C.-Y. Wu, H.-M. Cheng, and W.-F. Hsieh, Appl. Phys. Lett. **89**, 013101 (2006).

[6] A. Ohtomo, R. Shiroki, I. Ohkubo, H. Koinuma, and M. Kawasaki, Appl. Phys. Lett. **75**, 4088 (1999).

[7] H. Ryoken, N. Ohashi, I. Sakaguchi, Y. Adachi, S. Hishita, and H. Haneda, J. Cryst. Growth **287**, 134 (2006).

[8] Z. G. Ju, C. X. Shan, C. L. Yang, J. Y. Zhang, B. Yao, D. X. Zhao, D. Z. Shen, and X. W. Fan, Appl. Phys. Lett. **94**, 101902 (2009).

[9] J. L. Morrison, J. Huso, H. Hoeck, E. Casey, J. Mitchell, L. Bergman, and M. G. Norton, J. Appl. Phys. **104**, 123519 (2008).

[10] X. Du, Z. Mei, Z. Liu, Y. Guo, T. Zhang, Y. Hou, Z. Zhang, Q. Xue, and A. Yu. Kuznetsov, Adv. Mater. **21**, 4625 (2009).

[11] J. F. Sarver, F. L. Katnack, and F. A. Hummel, J. Electrochem. Soc. **106**, 960 (1959).

[12]S. O. Kucheyev, J. S. Williams, C. Jagadish, J. Zou, C. Evans, A. J. Nelson, and A. V. Hamza, Phys. Rev. B **67**, 094115 (2003).

[13]A. Yu. Azarov, S. O. Kucheyev, A. I. Titov, and P. A. Karaseov, J. Appl. Phys. **102**, 083547 (2007).

[14]R. Khanna, K. Ip, Y. W. Heo, D. P. Norton, S. J. Pearton, and F. Ren, Appl. Phys. Lett. **85**, 3468 (2004).

[15]V. A. Coleman, H. H. Tan, C. Jagadish, S. O. Kucheyev, and J. Zou, Appl. Phys. Lett. **87**, 231912 (2005).

[16]J. F. Ziegler, J. P. Biersack, and U. Littmark, *The Stopping and Range of Ions in Matter* (Pergamon, New York, 1985), Vol.1, p. 109; [www.srim.org].

[17]Y. Zhang, H. J. Whitlow, T. Winzell, I. F. Bubb, T. Sajavaara, J. Jokinen, K. Arstila, and J. Keinonen, Nucl. Instrum. Methods Phys. Res., Sect. B **149**, 477 (1999).

[18]M. S. Janson, *CONTES Instruction Manual*, Internal Report (Uppsala University, 2005).

[19]A. Yu. Azarov, B. G. Svensson, A. Hallén, X. L. Du, and A. Yu. Kuznetsov, J. Appl. Phys. **108**, 033509 (2010).

[20]The depth scale for the MgZnO films was calculated using the constant material density determined by a linear interpolation between the densities of ZnO (5.6 g/cm^3) and MgO (3.58 g/cm^3). However, the accuracy of this approach decreases in the near-surface region in panels (b) and (c) due to dramatic variations in stoichiometry.

[21]T. Ohsawa, N. Ohashi, Y. Adachi, I. Sakaguchi, H. Ryoken, K. Matsumoto, H. Haneda, S. Ueda, H. Yoshikawa, and K. Kobayashi, Appl. Phys. Lett. **92**, 232108 (2008).

[22]*CRC Handbook of Chemistry and Physics*, 84th ed., edited by D. R. Lide (CRC Press, New York, 2003).

[23]Note that it is not possible to quantify structural changes within ZnO buffer layer due to its small thickness, which is far below the RBS resolution.

[24]R. S. Wang and H. C. Ong, J. Appl. Phys. **104**, 016108 (2008).

[25]Note that some deviation from the increasing trend for the MgZnO samples implanted with 3×10^{16} Er/cm^2 may be attributed to the fact that these samples were annealed at 700 °C prior to 800 °C anneals.

[26]The implanted dopant profiles were calculated by convolution of depth profiles obtained by TRIM code (Ref. 16) simulation with a Gaussian function reflecting experimental smearing due to the limited depth resolution of RBS. The parameters of such a smearing Gaussian function were determined by fitting the slope of a RBS random spectrum.

[27]E. Rita, E. Alves, U. Wahl, J. G. Correia, T. Monteiro, M. J. Soares, A. Neves, and M. Peres, Nucl. Instrum. Methods B **242**, 580 (2006).

[28]E. Rita, E. Alves, U. Wahl, J. G. Correia, A. J. Neves, M. J. Soares, and T. Monteiro, Physica B **340-342**, 235 (2003).

[29]S. Sato, R. Takahashi, M. Kobune, and H. Gotoh, Appl. Catal. A **356**, 57 (2009).